Methodology for Fabrication-Tolerant Planar Directional Couplers

Choon Kong Lai, Yile Zhong, Wu Yi Chong, Duk-Yong Choi, *Member, IEEE*, Harith Ahmad, and Stephen Madden

***Abstract*—A new methodology for realizing fabrication-tolerant planar directional couplers is proposed and experimentally demonstrated. Performance of power splitting and WDM couplers can be made highly tolerant to typical process errors when an appropriate center-to-center spacing is chosen due to changes in the mode area compensating waveguide edge to edge variation along a very specific design locus. Using this approach, 2–3% index contrast waveguide couplers were fabricated and tested, demonstrating the predicted improved fabrication tolerances. High index contrast silicon-on-insulator systems are also shown to exhibit the same mechanism. The high fabrication tolerance demonstrated is of particular importance for vertically stacked hybrid integration of different materials platforms, where achieving tight critical dimension control over significant physical topology is problematic. Additionally the method will be of utility in circumstances where tight tolerances are required on coupling ratios such as coupled resonator filter devices etc.**

***Index Terms*—Directional couplers, tolerance analysis, integrated optics, optical device fabrication, lithography.**

I. Introduction

THE quest to build fully integrated optical systems requires the heterogeneous integration of multiple material systems onto a single chip, each chosen for their performance excellence in a particular sphere (passive, amplifying, nonlinear, electro-optic, detecting, etc). A simple approach to this is to vertically layer these material systems, using either width tapers [1], [2] or vertical tapers e.g., [3], [4] to interconnect the layers with low loss. As it is desirable to pattern the uppermost layers first as these have the smallest features, inevitably this leads to the formation of substantial surface topological variation from the processing of the upper layers that makes lithography for the bottom-most layer more difficult. Particularly, dimensional accuracy control of the bottom layer patterns becomes challenging due to varying photoresist thickness, topological reflections during exposure and other effects. Dimensional accuracy is critical to performance for many components, one particularly important device class being evanescent couplers. In evanescent devices, the field in the gap between the waveguides decays quasi-exponentially so a small error in the gap has serious performance consequences.

Various types of couplers (power splitters, tap monitoring couplers, wavelength multiplexing couplers, etc.) are needed in general circuits and in rare earth doped amplifier/laser devices. The challenge lies is how to relax lithography tolerances to a comfortable level for these different device types even in the presence of nonuniform photoresist films resulting from hybrid device topologies. In fiber-based directional couplers, light coupling can be monitored in real time during device fabrication to compensate any process issues, whereas planar integrated devices experience in-line non-correctable wafer scale random and systematic process variations which affect the final device geometry and hence the device performance. The typical errors include critical dimension (CD) errors in the photomask, lithographically induced CD variations in the etch mask (arising from exposure dose error and nonuniformity from interference/inhomogeneous reflection conditions where photoresist covers topology), and an etch bias relative to the actual size of the etch mask, all of which can vary across the surface of the wafer. Take one of the common photoresist AZ MIR 701 series as an example, the Bossung plots and dose-to-clear swing curve provided in the technical datasheet suggest that the critical dimension is very sensitive to the exposure dose, focus and the film thickness [5]. To illustrate, 0.1 μm CD variation can be induced by 25% change in the exposure dose at zero focus offset while a 1.2 μm resist thickness will require twice as much exposure dose as the 0.8 μm counterpart. These effects result in waveguide core width variation, leading to a random gap variance between the waveguide edges in a coupler that cannot be compensated by design alone. As the field varies quasi-exponentially in the gap between the cores, this leads to strong variations in the coupling between the waveguides in an

Manuscript received April 12, 2022; revised May 24, 2022; accepted May 28, 2022. Date of publication June 2, 2022; date of current version June 9, 2022. This work was supported in part by the Agilent Technologies through The Australian Research Council Linkage under Grant LP150100914, in part by UMRG under Grant RP029C-15AFR, in part by the joint grant between University of Malaya and the Australian National University, Malaysia Ministry of Education Long-term research under Grant LRGS(2015)/NGOD/UM/KPT, and in part by PPP research under Grant PG243-2016A. The work of Choon Kong was supported by the dual Ph.D. program scholarships from both UM and ANU. The work of Yile Zhong was supported by China Scholarship Council through the Ph.D. Scholarship under Grant 201606310180. (*Corresponding author: Choon Kong Lai.*)

Choon Kong Lai is with the Dual-Ph.D. Program, University of Malaya, Kuala Lumpur 50603, Malaysia, and also with the Dual-Ph.D. Program, The Australian National University, Canberra, ACT 2601, Australia (e-mail: laichoonkong@gmail.com).

Yile Zhong, Duk-Yong Choi, and Stephen Madden are with Quantum Science and Technology, Research School of Physics, The Australian National University, Canberra, ACT 2601, Australia (e-mail: yile.zhong@anu.edu.au; duk.choi@anu.edu.au; stephen.madden@anu.edu.au).

Wu Yi Chong and Harith Ahmad are with Photonics Research Centre, University of Malaya, Kuala Lumpur 50603, Malaysia (e-mail: wuyi@um.edu.my; harith@um.edu.my).

Digital Object Identifier 10.1109/JPHOT.2022.3179649

evanescent coupler device. However, it is important to note the waveguide core center to center separation defined on the mask is still very accurately transferred into the final device since errors in the waveguide width from the above effects are usually symmetric. Thus it is the width of the waveguides that is in fact the uncontrolled variable.

Given the importance of couplers in planar circuit implementations, the impact of these random uncontrollable errors is of considerable interest, as is the question of how it affects different coupler implementations. Various coupler implementations have been demonstrated such as multimode interference (MMI) couplers [6]–[8], directional couplers [9]–[13], unbalanced Mach-Zehnder interferometers (MZI) [14], [15] and (a)symmetric X and Y-branches [16], etc. Although all of the proposed methods have demonstrated good performance in terms of transmission and extinction ratio, there is relatively little published study on dimensional error tolerance. Among the devices mentioned, unbalanced MZIs themselves require high performance 3 dB couplers to function even before accounting for wavelength/phase errors resulting from small variations in the waveguide dimension while asymmetric Y-branches experience fabrication complexity when very low losses are required due to the presence of a vanishing point tip where the two branches meet at the "Y" section. MMI and directional couplers seem the more practical options from the fabrication tolerance perspective, and MMIs are generally considered to be quite fabrication tolerant at least for 3-dB couplers [17]–[19]. However, where insertion loss performance is paramount, evanescent couplers have a significant advantage as they are essentially just pieces of waveguide. Further, tight control of arbitrary coupling ratios and wavelength response is necessary for a range of high-performance optical devices, especially those utilizing ring resonator structure (e.g., coupled resonator optical waveguide filters), and fabrication tolerances are a significant challenge in such devices. Bogaerts *et al.* proposed a Monte Carlo simulation where the circuit performance and yield are evaluated through the thickness and width map of the wafer [20]. This report highlights the impact of the layout-aware variability on the optimized coupler performance but the technique for obtaining a dimensional tolerant design is missing. Thus, the question arises to whether there is any design optimization applicable to different types of couplers that can compensate the variations arising particularly in topographically challenging environments such as hybrid integrated circuits.

Study on this topic has been ongoing and there are two particularly relevant studies. Han, in his 2011 thesis, had first demonstrated a fabrication tolerant zone for $\sim$2% refractive index contrast symmetric directional couplers [21]. A locus was found where the coupling length was essentially constant for a useful range of waveguide widths as the center-to-center spacing was varied. Further it was shown that there is in fact only a single design that is both polarization independent and fabrication tolerant. In 2014, Mikkelsen *et al.* carried out a dimensional tolerance study on silicon-on-insulator (SOI) directional couplers [22]. It was shown that for high index contrast systems the core thickness is a critical parameter and there exist nearly stationary points where $\frac{\partial \Delta n}{\partial w} - \frac{\partial \Delta n}{\partial g} = 0$, where the Δn, w and g are the change in effective index, width and gap. Although a different approach was used in presenting the dimensional tolerances, the results agreed with Han's work demonstrating that the underlying principles also operate at high refractive index contrasts.

In this paper, a more comprehensive theoretical and experimental study is presented on all relevant types of symmetric directional coupler by further exploring the observed stationary points. Design guidelines for each type of coupler are outlined to enable minimum sensitivity to fabrication effects. In this study, width and center-to-center spacing are used as variables in quantifying the lithography performance for the reasons noted above and for having a waveguide spacing parameter that enables mask tolerance specifications that are independent of the device design/fabrication. Medium index contrast germanosilicate waveguides suitable for fiber butt coupling were studied here as the fiber compatibility, low loss and low nonlinearity make them natural candidates for the lowest layer of a vertically stacked structure where lithography control would be at its worst. Whilst waveguide core thickness accuracy and uniformity were shown to be critical for SOI devices, sufficient control and accuracy is possible via optical monitoring for physical and chemical vapor deposited materials to achieve even 0.1% tolerances [23], removing core thickness as a variable for these types of devices. Thus, it was not considered in the following study. Beyond insertion loss and coupling ratio, polarization dependence is also a critical performance parameter for many devices and has been investigated in this study.

II. Concept, Design and Modelling

Various representations of supermode and coupled mode theory for parallel dielectric waveguides have been established since the 1980s, e.g., [24], [25]. Here the supermode representation is exploited to gain detailed understanding of the fabrication tolerance dependence on design parameters. All waveguide structures considered here were modelled using the full vector modes of the Rsoft component design suite (comprising CAD layout, FEMSim finite element mode solver, BeamPROP 3D beam propagation solver). Fig. 1 (a) illustrates a pair of coupled parallel phase-matched (identical) waveguides with a sample cross sectional refractive index profile of a 3% index contrast germanosilicate waveguide. The waveguide height in the simulation was fixed at 3 μm because that is the largest allowable square geometry waveguide which operates in the single mode region at 3% index contrast in the 1.55 μm telecoms band. Fig. 1(b), (c) provide lateral cross sections for the dominant electric fields of the two lowest order, symmetric/even supermode (ESM) and anti-symmetric/odd supermode (OSM), generated using Rsoft FemSIM. The expression for coupling length required for light to travel half a cycle (power is completely cross coupled to the adjacent waveguide), L_π is given in eq. (1).

$$L_\pi = \frac{\lambda}{2(n_{effs} - n_{effa})} \tag{1}$$

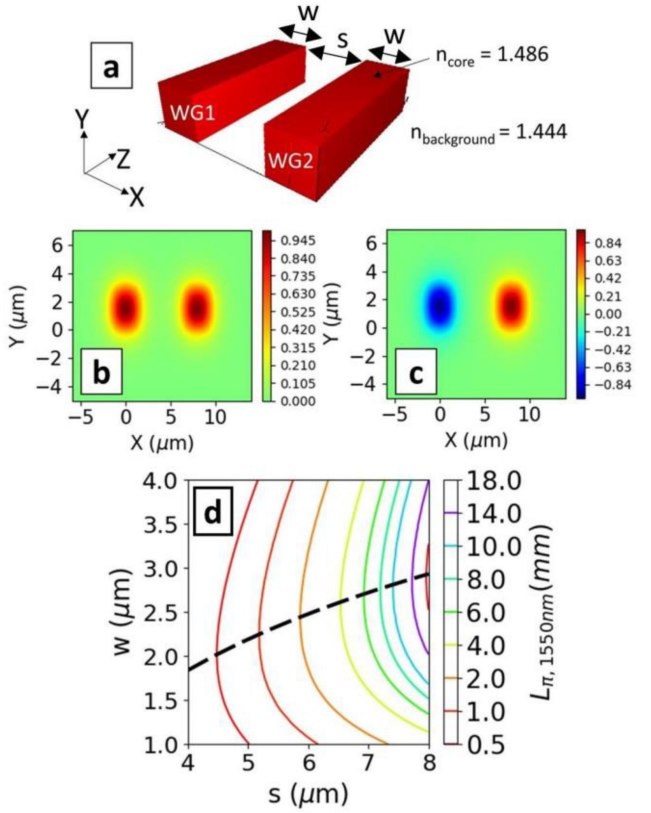

Fig. 1. (a) Model geometry where XY-plane is the waveguide cross section and Z is the light propagation direction; (b-c) intensity distribution of lowest order symmetric and anti-symmetric supermodes; (d) TE coupler length contour plot for full cross coupling parameterized with w and s. Black dashed line is the locus of maximum width tolerance.

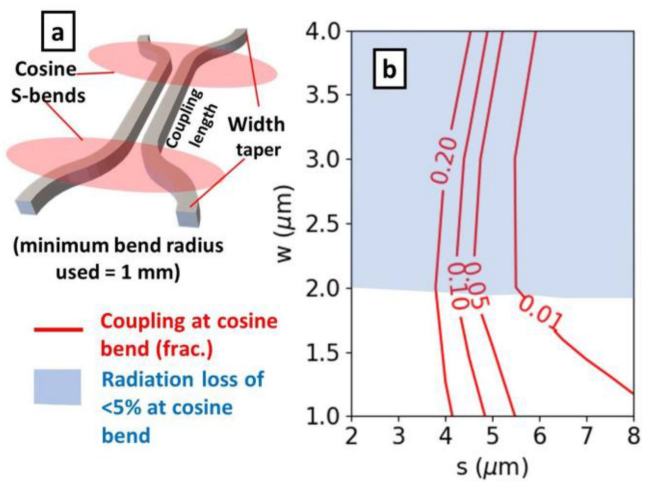

Fig. 2. (a) Illustration of parallel waveguides with cosine S-bends and width taper at the inputs (b) S-bends coupling and radiation loss versus w and s at 1550 nm.

where n_{effs} and n_{effa} are effective modal refractive indices of the ESM and OSM respectively. The effective indices of the ESM and OSM vary with wavelength, λ, waveguide width, w, and waveguide center-to-center spacing, s.

As noted, typical process variations result only in changes in waveguide width, whilst the waveguide center to center spacing is set solely by the photomask (which itself may have small errors). Changing the width of the waveguide changes its field distribution and modal area. In principle, by altering the width, any optical waveguide operating in the fundamental mode can exhibit a minimum mode volume behavior (refer to Fig. 1(b) of [26]) where to the left of the minimum, more power spreads into the cladding rapidly increasing the mode size, and to the right, more power concentrates in the larger core increasing the field size at a slower rate. The area where a small change in the mode area occurs around the minimum point is predicted to yield a small change in the overlap integral and coupling strength between the two parallel waveguides, and eventually leading to a more fabrication tolerant coupler. To verify the existence of such minimum behavior in the parallel waveguides, a parametric study of the coupler performance with varying w and s at wavelengths of interest was carried out.

The contour plot of Fig. 1(d) was generated by varying w and s in 50 nm increments, to compute the L_π for both TE and TM modes (TE shown). The contour lines represent the {w, s} pairs providing full cross over coupling for particular coupler lengths not exceeding 20 mm i.e., practically sized couplers. The salient point from Fig. 1(d) is that the contour line for any chosen coupling length has a single center-to-center spacing where the tangent to the contour is a vertical line, i.e., the width does not affect the coupling length locally. This is precisely the condition to maximize tolerance to the waveguide width and verifies that the proposed compensation mechanism is present. The locus of the optimum points is represented by the black dashed line drawn on Fig. 1(d) for TE modes, and for a fully polarization independent coupler the intersection of the TE and TM minimum sensitivity loci is the optimum design. However there is only a single point that is fully polarization independent, and consequently birefringence effects are more fully considered in following sections.

A. *Addition of S-Bend*

The illustration above for a pair of parallel waveguides is not a practical device. S-bends and width tapers are required at the ends of the parallel waveguides to terminate evanescent wave coupling. For a 3% index contrast system, cosine S-bends with 1 mm minimum radius and 4.2° final angle were used as shown in Fig. 2(a).

Setting the parallel waveguide length to zero, the S-bend cross coupling and loss for different w and s can be determined. From Fig. 2(b), as s reduces, the coupling from the S-bends increases rapidly and may significantly shift the tolerant zone (black dashed line) as indicated in Fig. 1(d). This requires either correcting the contour plot of Fig. 1(d) to include the S-bend coupling or avoiding the regions of (w, s) where the S-bend coupling exceeds ~5%. The latter approach was taken because the former requires significant amounts of time-consuming BPM based computation. Further, reducing w increases the S-bend loss, therefore the blue region ($w \geq 2$ μm for > 0.95 transmission) is the optimum choice.

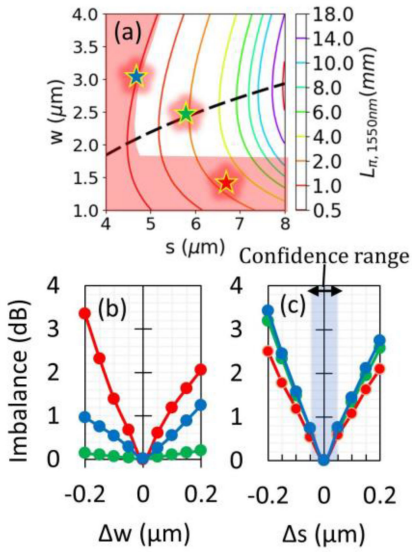

Fig. 3. (a) 3-dB coupler tolerance analysis: (a) Position of modelled designs on the w-s contour plot; (b) imbalance vs width deviation, (c) imbalance vs center-to-center spacing deviation.

B. Dimensional Tolerance Analysis of 3-dB Coupler

A 3-dB coupler requires a length of $L_{\pi/2}$. The two parameters that determine the performance of a 3-dB coupler are the power imbalance and excess loss (EL), defined in eq. (2) and eq. (3) respectively. Both quantities should be minimized.

$$P_{imbalance}\ \ (dB) \ = \ \left| 10 \times \log_{10}\left(\frac{P_{Bar\ port}}{P_{Cross\ port}}\right)\right| \tag{2}$$

$$EL\ \ (dB) \ = \ 10\ \times \log_{10}\left(P_{Bar\ port} + P_{Cross\ port}\right) \tag{3}$$

where $P_{Bar\ port}$ and $P_{Cross\ port}$ are the power at the bar (through) port and cross port respectively. To compare the fabrication tolerances between designs on the black dashed line of Fig. 1(d) and more arbitrary design choices, three designs were selected for the subsequent tolerance analysis using the full vector beam propagation method (BPM) model. The selected designs are marked on the contour plot in Fig. 3(a). Note that the red zone drawn on the plot is representing S-bend radiation loss and crosstalk of >5% as previously.

BeamPROP simulations were carried out for these designs with design variation of ± 0.2 μm, simulating a reasonably generous CD tolerance, one certainly achievable with low cost lithography tools under normal circumstances or I line type steppers/scanners where resist inhomogeneity is present. The results are plotted in Fig. 3(b)-(c). All the designs have low excess loss (<0.03 dB) and Fig. 3(b) shows that the optimized design (labelled green) is indeed tolerant to the modelled CD variation. The non-optimized devices (blue and red), display performance that is quite sensitive to width variation, noting that 0.3 dB imbalance is required to achieve 30 dB extinction in a Mach-Zehnder interferometer (ie +/- 50nm for the blue plot), and 0.1 dB for 40 dB (about +/-15nm for the blue plot). In terms of Δs, Fig. 3(c) illustrates the sensitivity is far greater for all designs with only marginal differences in sensitivity to variation. As noted previously, this parameter is set only by the photomask fabrication which is a once off shared cost and so can be mitigated with sufficiently accurate (expensive) mask fabrication (+/−50 nm CD tolerance is commercially available on 1x laser written masks) or reduction lithography (on wafer mask CD tolerance of less than +/− 15 nm).

Polarization induced coupling variations and power crosstalk/incomplete coupling can be calculated from the solution to the coupled mode equations for synchronous waveguides ie no propagation constant mismatch ($\Delta\beta = 0$) [27], which has a cosine squared functional relationship with length divided by length for complete cross over. The polarization dependent loss for one power crossing is given in eq. (4). To provide quantitative insight, the TM cross and bar port transmission were computed for five equi-spaced points along the maximum TE tolerance locus of Fig. 3(a). The TM imbalance varied essentially linearly from zero at s = 8 μm to 0.3 dB at s = 4 μm.

$$PDL\ per\ crossings\ \ (dB) \\ = \ -10.\ \log_{10}\left[\cos^2\left(\frac{\pi}{2}.\ \frac{|L_{\pi,TE} - L_{\pi,TM}|}{L_{\pi,TE}}\right)\right] \tag{4}$$

C. Dimensional Tolerance Analysis of WDM Coupler

The design mechanism for a wavelength splitter is almost identical to that of the power coupler discussed in the last section but with the consideration of two wavelengths. In general, mode area increases with wavelength when devices are not significantly sub-wavelength in cross section, and so the coupling coefficient of a longer wavelength is therefore higher than its shorter counterpart at a fixed *w* and *s*. Beat length is therefore smaller at longer wavelengths. eq. (5) defines the ratio Γ of beat length at λ_1 to the beat length at λ_2:

$$\mathbf{\Gamma} \ = \frac{L_{\pi\lambda_1}}{L_{\pi\lambda_2}} \tag{5}$$

where $L_{\pi\lambda_1}$ and $L_{\pi\lambda_2}$ are the length required for λ_1 and λ_2 ($\lambda_1 < \lambda_2$) to cross-couple respectively. To have a WDM coupler, λ_1 must couple an odd number of half cycles more than λ_2 such that the wavelengths exit separate ports. The simplest design can be obtained by choosing a combination of width and space that yield $\Gamma >> 2$, followed by $\Gamma = 2, 1.5, 1.33, 1.25$ etc. This is because for the case $\Gamma >> 2$, the difference in coupling coefficients is great enough that λ_1 essentially does not couple significantly to the adjacent waveguide, instead remaining in the input waveguide. The demultiplexing mechanism for a few selected values of Γ is summarized in Table I.

Generically it would be expected that a value of $\Gamma >> 2$ would give the most fabrication tolerant response as it prohibits the cross coupling for the shorter wavelength and the width sensitivity is solely dependent on the longer wavelength. Exactly what constitutes sufficiency in $\Gamma >> 2$ is evaluated by checking the cross coupling of λ_1 via the square of cosine function [27]

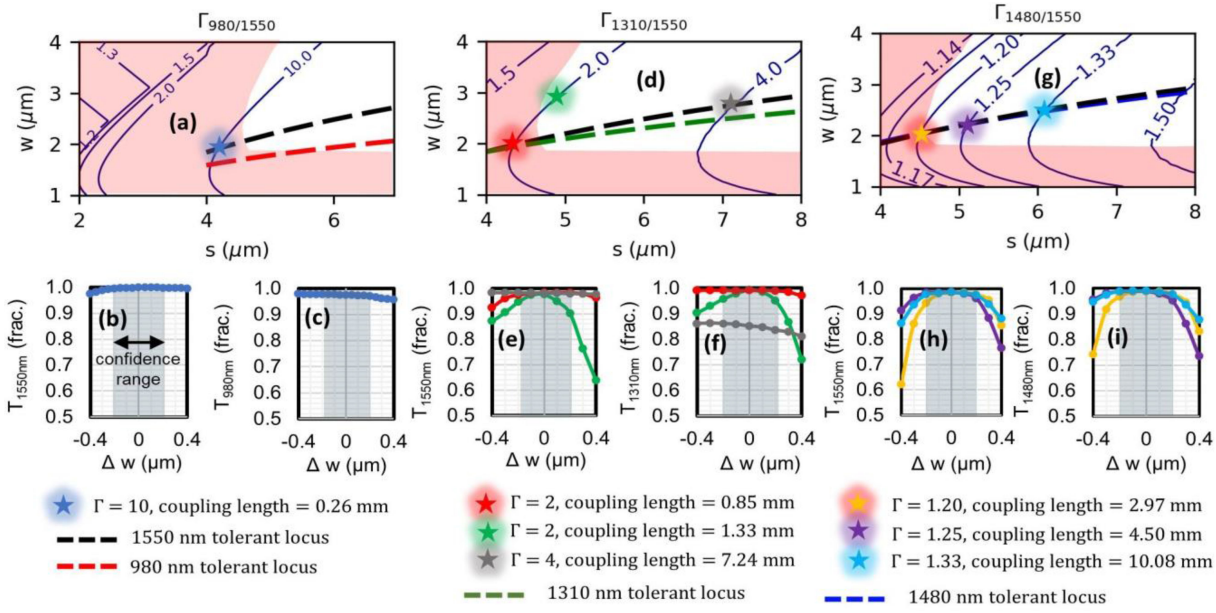

Fig. 4. (a) Contour map showing the possible Γ values for splitting 980 nm and 1550 nm. The red zone represents >5% cross coupling and loss at the S-bends; (b) graph of 1550 nm transmission versus the width deviation; (c) graph of 980 nm transmission versus the width deviation; (d) Contour map showing possible Γ values for 1310/1550 nm couplers and the corresponding (e) 1550 nm transmission vs width error and (f) 1310 nm transmission vs width error; (g) Possible Γ values for 1480/1550 nm coupler and the corresponding (h) 1550 nm transmission vs width error and (i) 1480 nm transmission vs width error. The dashed lines are the maximum tolerance loci where red, green, blue, and black color represents 980 nm, 1310 nm, 1480 nm, and 1550 nm wavelength respectively.

TABLE I
ENERGY TRANSFER MECHANISM AT λ_1 AND λ_2 ($\lambda_1 < \lambda_2$) FOR DIFFERENT Γ FOR INPUT AT WAVEGUIDE WG1

Γ	N_{λ_1}	N_{λ_2}	λ_1 OUTPUT PORT	λ_2 OUTPUT PORT
Γ >>2	0	1	WG1	WG2
Γ = 2	1	2	WG2	WG1
Γ = 1.5	2	3	WG1	WG2
Γ = 1.33	3	4	WG2	WG1

N_{λ_1} and N_{λ_2} denote the number of cross couplings occur for λ_1 and λ_2 respectively.

recast in Γ as eq. (6):

$$P_{\lambda 2} = 1 - P_{\lambda 1} = \cos^2\left(\frac{\pi}{2\Gamma}\right) \tag{6}$$

At Γ = 4 the crosstalk is 15% whereas Γ = 8 yields a crosstalk of 4% (ie. an insertion loss of 0.18 dB for the through light). FemSIM scans were performed across a range of w and s for a few chosen wavelengths of common interest (980 nm, 1310 nm, 1480 nm and 1550 nm). The choice of Γ, or more specifically the number of cross couplings, also impacts on the polarization dependent loss (PDL) of the device. The TE and TM coupling lengths differ across the {w, s} space and between wavelengths, meaning the port transmission cosine squared curves have slightly different periods. The TE and TM cross and bar coupling lengths therefore diverge more and more with increased cycle count leading to increasing loss for the TM mode if the device is designed on TE data. The choice of Γ, PDL and tolerance results for various types of WDM couplers will be discussed in the following subsections.

1) 980/1550-nm WDM Coupler: The computed contour map in Fig. 4(a) provides detailed information for obtaining the optimum tolerant 980/1550-nm coupler design. Note that the Γ contour lines do show similar trend with the coupling length contour of Fig. 1(d) for example, where there exist turning points ($d\Gamma/dw = 0$). However, these turning points are not the locus of interest for yielding tolerant WDM couplers. In other words, at those turning points, the coupling length may vary significantly with the width deviation. Hence, two dashed lines from the calculated coupling length contour plot corresponding to the two wavelengths of interest are overlaid on the Γ contour plot that actually represent the loci of maximum tolerance. As noted in Fig. 4, while the maximum tolerance loci are wavelength dependent, they approach each other as *s* decreases. A tolerant design can either be chosen from the red or black tolerant locus depending on the specific application. In our study, the dimensional tolerance is optimized at 1550 nm wavelength as it is the signal wavelength in most applications. Hence, the three criteria for the best coupler design here are: (1) avoiding the red zone where bend losses and coupling in the bends occurs; (2) lying on the tolerant locus (the black dashed line) and; (3) opting for the smallest possible s for realizing miniaturized couplers subject to polarization induced loss specifications.

Within the range of dimensions shown, obtaining $\Gamma_{980/1550} >> 2$ is easy for the 980/1550 nm WDM coupler. On the other hand, other $\Gamma_{980/1550}$ options such as Γ = 2, 1.5, 1.33, 1.25 are relatively far inside the red zone as well as being very close to each other, making them potentially sensitive to changes in s in particular. Therefore, a point marked with a Royal blue star lying on $\Gamma_{980/1550} = 10$ (Fig. 4(a)) was chosen for the simulation to minimize length and the separation of the 980 nm and 1550 nm

wavelength tolerant locus. Another advantage of choosing this point is that a low PDL can be obtained for both the 980 and 1550 nm (<0.01dB). Furthermore, as shown in Fig. 4(b), (c), both 1550 nm and 980 nm have <0.1 dB loss for $\Delta w = \pm 0.4$ μm, twice the likely fabrication tolerances. The design is thus extremely robust.

2) 1310/1550-nm WDM Coupler: As plotted in Fig. 4(d), the maximum $\Gamma_{1310/1550}$ contour contained within the simulation domain for a 1310/1550-nm coupler is at a value of 4. In total, there are three potential $\Gamma_{1310/1550}$ in the domain, which are $\Gamma_{1310/1550} = 4$ (>2), 2, and 1.5. The $\Gamma_{1310/1550} = 1.5$ contour line does not intersect with the tolerant locus (black dashed line), and hence all the 1310/1550-nm couplers operating at $\Gamma = 1.5$ are expected to be sensitive to the width deviation.

Therefore, two designs (marked red and grey) on the locus were chosen for tolerance analysis (see Fig. 4(d)). Also, one extra point marked green was chosen for comparison. The 1550 nm performance is shown in Fig. 4(e), both optimized designs (red and grey) have excess loss < 0.1 dB within the tolerance range whereas the loss value for the unoptimized design (green) reaches 0.5 dB at $\Delta w = 0.2$ µm. The 1310 nm transmission in Fig. 4(f) shows a similar trend to the 1550 nm data but with a lowered transmission for the $\Gamma_{1310/1550} = 4$ design. The transmission reduction is expected as per crosstalk estimation from eq. (6). Thus, the $\Gamma_{1310/1550} = 2$ is the preferred design for 3% index contrast 1310/1550-nm WDM coupler. Furthermore, it also lies on both 1310 nm and 1550 nm tolerant locus simultaneously, with a calculated <0.02 dB PDL for both wavelengths and a compact 0.85mm parallel waveguide length.

3) 1480/1550-nm WDM Coupler: When λ_1 and λ_2 are close to each other, the coupling strengths are very similar, and this makes obtaining $\Gamma >> 2$ within a short coupling length impractical at least for the studied 3% index contrast system. The number of energy exchanges must be increased to keep the coupling length short. As Fig. 4(g) shows, the highest operational Γ in the domain is 1.5.

Three designs were chosen on the maximum tolerance locus outside the red zone, labelled yellow, purple and light blue (Fig. 4(g)). From Fig. 4(h), (i), all designs exhibit excellent performance, having excess loss of < 0.2 dB within the tolerance range. Considering only coupling length, the $\Gamma = 1.20$ (yellow) design is preferred. The PDLs of the three designs increase with decreasing Γ due to the large number of cycles, being 0.19 dB for $\Gamma = 1.20$, 0.11 dB for $\Gamma = 1.25$, and 0.04 dB for $\Gamma = 1.33$. The best design choice then depends upon the application requirements.

D. Dimensional Tolerance Analysis of Tap Couplers

Couplers with low splitting ratios such as 95:5 are widely used for power monitoring. The coupler length required for 5% cross port power transfer is calculated from eq. (6) as one eighth of L_π. The design contours are shown in Fig. 5(a).

A simulation was carried out for two points labelled green and red on Fig. 5(a) for a 95:5 tap coupler. Both designs were chosen from the same contour line with a parallel waveguide length of 900 μm. The coupler performance with respect to

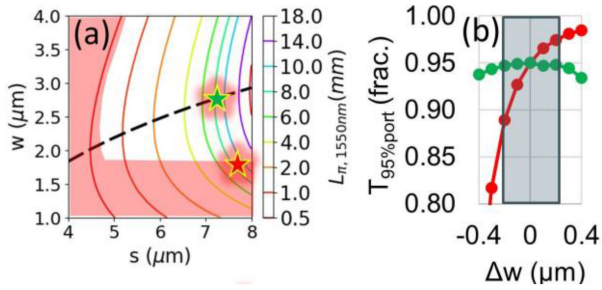

Fig. 5. (a) Design contours for 95:5 tap coupler at 1550 nm (b) Transmission at the 95% port vs the width error.

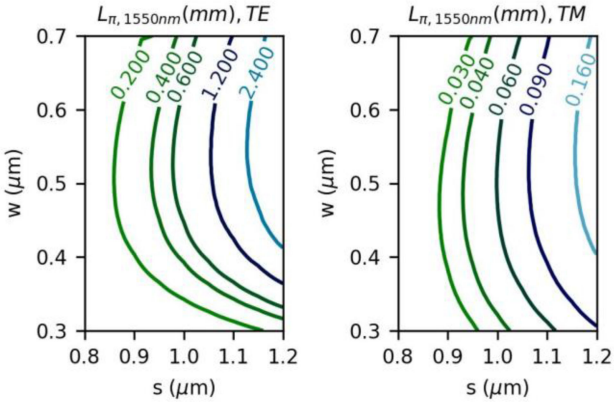

Fig. 6. Contour plot of coupler beat length vs w and s for 220 nm high by 550 nm wide SOI nanowire when the polarization state is (a) TE- and (b) TM-.

Δw is shown in Fig. 5(b). Note that the excess loss is very small and so the 5% port result is not shown in the figure but is one minus the bar port. The tolerant design (green) shows an almost perfect flat response ($\delta T/\delta w \approx 0$) over the tolerance window whereas the unoptimized design (red) experiences a significant deviation from 95% transmission in the presence of width change. Polarization effects are minimal due to the very short device length, with the zero width error TM bar port transmission response varying essentially linearly from 0.950 at $s = 8$ μm to 0.952 at $s = 4$ μm along the maximum tolerance locus.

E. Higher Index Contrast System

To illustrate that the compensation mechanism is not restricted to moderate index contrast systems, a study was carried out for high index contrast fully etched nominally 550 nm wide by 220 nm high silicon-on-insulator (SOI) waveguides and the results for both polarization states are plotted in Fig. 6.

The data of Fig. 6. indicate that SOI couplers are highly birefringent where the coupling lengths for TE- are of one order of magnitude higher than that of the TM- polarization state within a similar dimensional range; unsurprising when the basic waveguide is highly birefringent. However the results show that there still exists a locus of maximum insensitivity to width changes just as the lower index contrast system did. To illustrate, by referring to Fig. 6, a width tolerance of a few tens of nm can be achieved provided the parallel waveguides are accurately

spaced, which is several times more tolerant than the ~10 nm reported in the MZI with the bent directional couplers on SOI platform [28], [29]. It is noted that SOI is about the highest index contrast system in use today and so this establishes that all intermediate index contrast systems are likely have the same behavior. The sensitivity of effective index towards dimensional variation increases with the index contrast of a system. This explains why the contour line for lower index contrast systems (see Fig. 1(d)) is much flatter.

Regarding this issue, Mikkelsen *et al.* [22] proposed the use of rib SOI couplers to reduce the index contrast for improving the fabrication tolerance. However, this is just another trade off as the introduction of the "etch depth" parameter in the rib structure provides another source of fabrication error. Despite the issues with the birefringence and dimensional variation tolerance in the high index contrast system, this work at least shows the existence of a single maximum width-tolerant point for each center-to-center spacing used.

III. Experimental Demonstration of a Fabrication Error Tolerant Couplers

A. Device Fabrication and Measurement

The device designs resulting from the above discussion were implemented on chip using two different technologies. The first used 2%-Δ polysiloxane system [30], [31] and the second a 3%-Δ Ge-doped silica films. The polysiloxane system was used to demonstrate 3dB and 1310/1550 nm WDM couplers, and the germanosilicate for 980/1550 nm WDM.

The polysiloxane waveguides were fabricated by UV nanoimprinting [30], [31]. The UV-curable polysiloxane resin for the core had an index of 1.509, and the cladding 1.478 at 1550 nm. The 3% index contrast germanosilicate waveguides comprised of a core index of 1.486 and cladding index of 1.444 at 1550 nm were fabricated using flame hydrolysis deposition (FHD) and reactive ion etching (RIE). Instead of silica, ZPU UV curable polymer was used as the upper cladding material to make the fabrication process simpler as gap filling in the coupler region is then guaranteed. Photomasks for 1x lithography were fabricated at Taiwan Mask Corporation with a $\pm$50 nm tolerance on waveguide center-to-center spacings, and a variety of waveguide widths in order to be able to test out the resilience of the designs to waveguide width changes. After fabrication, it was found that the sidewall angle on both waveguide types was less optimal than expected, having an 82-degree slope.

The measurements were carried out using fiber butt-coupling with Nufern UHNA-3 fibers which offered very good matching with the 2%-Δ polysiloxane and 3%-Δ germanosilicate waveguides. With the aid of index matching fluid ($n = 1.486$), negligible fiber-to-waveguide coupling loss was anticipated. UHNA-3 has an operating wavelength range of 960–1600 nm, which is also therefore suitable for measurements between both 980 nm and 1550 nm. As verification of low coupling losses, the measured fiber-to-fiber insertion loss of a 7 mm long straight germanosilicate waveguide was 0.11 dB, compared to the expected polymer absorption limited propagation loss of 0.15 dB/cm if the fiber to coupling loss was negligible.

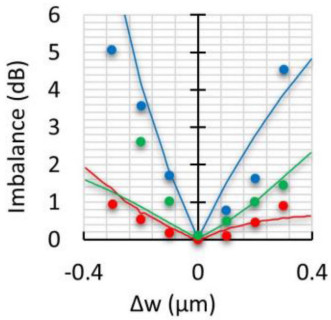

Coupler length (μm)	w (μm)	s (μm)
4652	3.3	8.6
2743	2.0	8.6
3681	4.5	8.6

Fig. 7. Simulated (solid lines) and measured (dots) power imbalance with waveguide sidewall angle of 83°.

B. Experimental Results

1) 3-dB Couplers: The optimized waveguide width, coupling length and core separation for 3-dB coupler in the birefringence-free 2%-Δ polysiloxane system were found to be 3.3 μm, 4652 μm, 8.6 μm respectively. The S-bend used in this case has a radius of 8005 μm with a final angle of 2.86°. Couplers with Δw of $\pm$0.4 μm were designed to investigate the width error tolerance. Two other width-sensitive designs (non-optimized devices as described in Section II.B) were also selected for comparison purposes. Fig. 7 illustrates the experimental results compared to a modified simulation for the actual fabricated waveguide profile noted above. The measurement were repeated several times for different sets of devices and the measurement errors in the imbalance are within 0.1 dB.

Imbalance $<$0.1 dB for $\pm$0.2 μm Δw was predicted for vertical sidewall couplers (see Fig. 3(b)), though as Fig. 7 shows, the sidewall angle has a significant impact on the quality of the width error compensation with 0.1 dB imbalance only achieved over $\Delta w = \pm$ 0.1 μm for the optimized design. Reasonable agreement was obtained between the experimental results and the measurements once the sidewall angle was accounted for as indicated in Fig. 7, confirming that the optimized coupler design is indeed the most fabrication tolerant. Further simulations indicated the sidewall angle must exceed 87° to recreate the performance of Fig. 3(b), which can be achieved by optimizing the lithography and etching processes. The angle was found to have such a significant effect as it directly affects the waveguide modal propagation constants and also induces birefringence.

2) 1310/1550 Nm Couplers: 1310 nm/1550 nm WDM couplers with 2% index contrast and $\Gamma = 2$ were fabricated. The error tolerant design in this case was 5.18 μm core separation and 2.25 μm core width. By comparison, two other designs were also selected from the same contour curve ($\Gamma = 2$); one used a waveguide width of 1.5 μm and the other 3.2 μm. The experimentally measured results for the above couplers are shown in Fig. 8(a) and (b).

At 1550 nm (Fig. 8(b)), the extinction ratio follows the predictions of the modeling. The optimized design was tolerant to an error of $\pm$300 nm in waveguide width for $>$30 dB power extinction ratio and was far superior to the un-optimized designs. At 1310 nm the performance was much poorer with an extinction

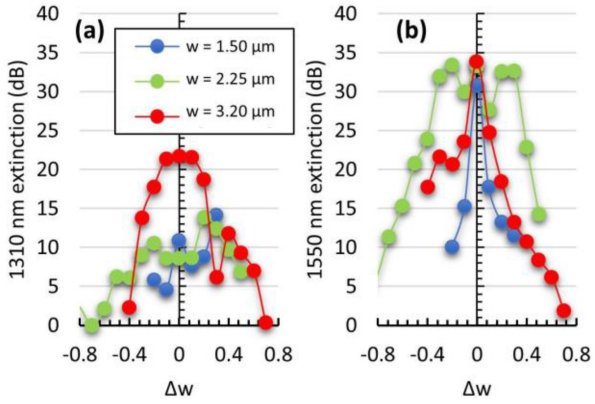

Fig. 8. Measured extinction for the imprinted WDM couplers (a) 1310 nm (b) 1550 nm.

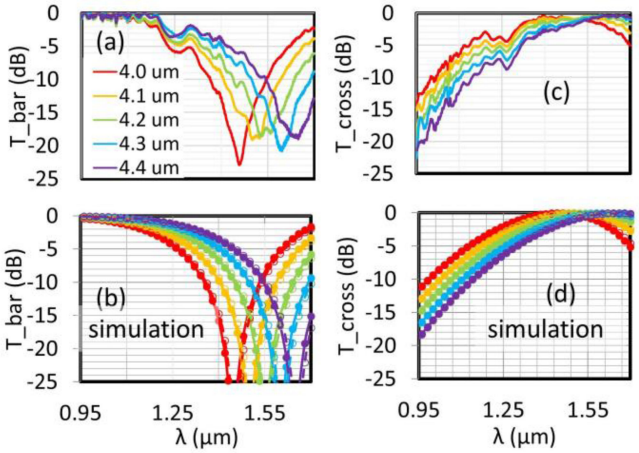

Fig. 9. (a) Experimental (b) simulated bar port transmission spectrum and (c) experimental (d) simulated cross port transmission spectrum. Nominal design separation is 4.2 μm. The different color used represent different center-to-center spacing as shown in the legend. The solid lines and dashed lines in the simulation graph represent TE- and TM-polarization.

ratio of only around 10 dB though relatively invariant with width changes. Spectrally resolved measurements showed that the transmission minima wavelengths were exactly aligned to the design values indicating that the basic coupler design was correct. However, the low extinction ratios at the cross-port indicated that the coupling was imperfect. It is well known that to obtain full cross over coupling from one waveguide to another, the two waveguides must have identical propagation constants. Any small difference between the coupling waveguide dimensions can result in a phase mismatch and this leads to incomplete coupling and power remaining in the input waveguide, e.g., [32].

Simulations of a coupler indicated a 0.00005 difference in the effective index between the two waveguides could produce the observed reduction in extinction ratio at 1310 nm whilst it had a negligible effect on performance at 1550 nm. Such a small difference could result if the core widths differed by as little as 20 nm. As this was below the photomask CD specification, the performance reduction likely originated from an inaccuracy on the mask itself. This problem is common to any WDM coupler structure and unfortunately manifested on the optimized version of the coupler to a degree obscuring the width tolerance at 1310 nm.

IV. Discussions

With the experimental verification, further insight can be gained from the results of dimensional tolerance analysis to formulate a general rule-of-thumb in designing planar directional couplers. First of all, we showed that the width tolerant loci – the dashed lines – are one-to-one continuous functions when plotted on a w-s plane regardless of the index contrast of the waveguide platform. This means a less simulation effort is required to determine the tolerant loci. To illustrate, a parameter sweep of width can first be performed at a several reasonable center-to-center spacings, instead of fine sweeping the center-to-center spacings. Then the tolerant loci are formed by connecting all the points that has minimum change of L_π. In fact the tolerant loci of waveguide height can also be determined using similar approach.

It is also noteworthy that, unlike widths, there does not exist a clear tolerant zone for center-to-center spacing from Fig. 1(d). However, there is a general trend that L_π increases nonlinearly with spacing, meaning a higher spacing-tolerance is anticipated at a smaller spacing. In this paper, a statement was made with regards to the center-to-center spacing that it is set solely by the photomask. While the spacing error should not be a concern given the high-end photomask manufacture can typically achieve a spacing uncertainty of $\pm$50 nm, it is interesting to examine the impact of spacing on the coupler performance at the best possible spacing-tolerant point. Therefore a 980/1550 nm WDM couplers with $\Gamma = 10$ (coupling length $= 260$ μm, width $= 1.9$ μm) were fabricated in the 3%-Δ Germanosilicate system to investigate the Δs dependence. This design, as illustrated in Fig. 4(a), lies on the width tolerant locus, and having the best possible spacing-tolerance outside of the red zone. Couplers with center-to-center spacings of 4.0, 4.1, 4.2, 4.3, and 4.4 μm were included in the photomask (4.2 μm nominal design). Spectrally resolved measurements were performed on the fabricated devices. Both experimental and simulation results for TE- and TM-polarization states are shown in Fig. 9.

The agreement between simulation and experiment is very good. In terms of device tolerance, isolation of >15 dB and low transmission loss at 1550 nm can be obtained with $\Delta s = \pm 0.1$ μm. Similar results can also be observed for 980 nm coupling. The center-to-center spacing sensitivity is acceptable with an appropriately toleranced photomask at $+/-0.1$ μm CD (and even more so if reduction projection lithography were to be used with this reducing mask dimensional error by 4-5x or more with the higher end mask writes typically used for stepper reticles). Again small differences in the waveguide core widths manifest in the bar port responses limiting the extinction at 1550 nm.

Finally, a general design protocol of planar directional coupler can be summarized as follow:

1. Perform a width scan at a several spacing to determine the point where a minimum change of L_π occurs, followed by connecting these points to form a width-tolerant locus. Choosing a reasonable {w,s} domain can reduce the simulation effort significantly.

2. Define a "red-zone" where the S-bends added have radiation loss or crosstalk of >X. The X used in this work is 5%. The simulation results can be improved by further lowering the X.
3. Select a design with a {w, s} pair lying outside of the red zone, sitting on the width-tolerant locus with the smallest possible center-to-center spacing.
4. For wavelength (de-)multiplexers, repeat the steps above with another wavelength of interest, then compute the ratio Γ within the same {w,s} domain. Then the best design is selected if it sits on the width-tolerant locus and one of the allowable Γ (>>2, 2, 1.5, 1.33, etc.) simultaneously outsife the red zone defined in step 2.

V. Conclusion

A new general design methodology for planar waveguide directional couplers was proposed, numerically tested and experimentally demonstrated to maximize fabrication error tolerance in power splitting and WDM couplers. Whilst of utility in improving device yield generally, the results are of particular importance for multi-material system single chip hybridized devices where lithography has to be undertaken in the presence of significant physical topography, considerably increasing the difficulty of maintaining tight dimensional control.

Acknowledgment

The equipment and process access through the Australian National Nanofabrication Facility ACT node and ANFF OptoFab ACT node is also gratefully acknowledged.

References

[1] Y. Maegami *et al.*, "Spot-size converter with a SiO_2 spacer layer between tapered Si and SiON waveguides for fiber-to-chip coupling," *Opt. Exp.*, vol. 23, no. 16, pp. 21287–21295, 2015.

[2] T. Tsuchizawa *et al.*, "Microphotonics devices based on silicon microfabrication technology," *IEEE J. Sel. Top. Quantum Electron.*, vol. 11, no. 1, pp. 232–240, Jan./Feb. 2005.

[3] S. Madden, Z. Jin, D. Choi, S. Debbarma, D. Bulla, and B. Luther-Davies, "Low loss coupling to sub-micron thick rib and nanowire waveguides by vertical tapering," *Opt. Exp.*, vol. 21, no. 3, pp. 3582–3594, 2013.

[4] C. K. Lai *et al.*, "Hybrid chalcogenide-germanosilicate waveguides for high performance stimulated brillouin scattering applications," *Adv. Funct. Mater.*, vol. 32, no. 3, 2021, Art. no. 2105230.

[5] "AZ MIR 701 technical datasheet," Accessed: Jun. 4, 2021. [Online]. Available: https://www.microchemicals.com/micro/tds_az_mir701_photoresist.pdf

[6] W. L. Jung, W. J. Lee, H. L. Tae, Y. J. Myung, B. G. Kim, and B. S. Rho, "Polymer-based wavelength multi/demultiplexer using multimode interference," in *Proc. Joint Conf. Opto-Electron. Commun. Conf. Australian Conf. Opt. Fibre Technol.*, 2008, pp. 1–2.

[7] M. R. Paiam, C. F. Janz, R. I. MacDonald, and J. N. Broughton, "Compact planar 980/1550-nm wavelength multi/demultiplexer based on multimode interference," *IEEE Photon. Technol. Lett.*, vol. 7, no. 10, pp. 1180–1182, Oct. 1995.

[8] A. Bakhtazad, J. McMullin, C. Haugen, and R. Decorby, "MMI multiplexer for dual-channel erbium-doped waveguide amplifiers," *Opt. Exp.*, vol. 9, no. 4, pp. 178–183, 2001.

[9] K. Hattori, T. Kitagawa, M. Oguma, Y. Ohmori, and M. Horiguchi, "Erbium-doped silica-based waveguide amplifier integrated with a 980/1530 nm WDM coupler," *Electron. Lett.*, vol. 30, no. 7, pp. 856–857, 1994.

[10] C. Kim *et al.*, "Robust, low-noise, polarization-maintaining mode-locked Er-fiber laser with a planar lightwave circuit (PLC) device as a multi-functional element," *Opt. Lett.*, vol. 42, no. 8, pp. 1472–1475, 2017.

[11] J. H. Song *et al.*, "Bragg grating-assisted WDM filter for integrated optical triplexer transceivers," *IEEE Photon. Technol. Lett.*, vol. 17, no. 12, pp. 2607–2609, Dec. 2005.

[12] J. H. Song *et al.*, "Thin film filter-embedded triplexing-filters based on directional couplers for FTTH networks," *IEEE Photon. Technol. Lett.*, vol. 17, no. 8, pp. 1668–1670, Aug. 2005.

[13] A. W. P. Law, W. Y. Chong, F. R. M. Adikan, and H. Ahmad, "Modeling of 980/1550nm PLC WDM directional coupler," in *Proc. IEEE 6th Nat. Conf. Telecommunication Technol. IEEE 2nd Malaysia Conf. Photon.*, 2008, pp. 6–11.

[14] N. Feng *et al.*, "Low-loss polarization-insensitive silicon-on-insulator-based WDM filter for triplexer applications," *IEEE Photon. Technol. Lett.*, vol. 20, no. 23, pp. 1968–1970, Dec. 2008.

[15] T. Lee, D. Lee, and Y. Chung, "Design and simulation of fabrication-error-tolerant triplexer based on cascaded Mach-Zehnder inteferometers," *IEEE Photon. Technol. Lett.*, vol. 20, no. 1, pp. 33–35, Jan. 2008.

[16] T. Negami, H. Haga, and S. Yamamoto, "Guided-wave optical wavelength demultiplexer using an asymmetric *Y* junction," *Appl. Phys. Lett.*, vol. 54, no. 12, pp. 1080–1082, 1989.

[17] R. Halir *et al.*, "A design procedure for high-performance, rib-waveguide-based multimode interference couplers in silicon-on-insulator," *J. Lightw. Technol.*, vol. 26, no. 16, pp. 2928–2936, Aug. 2008.

[18] H.-D. Kenchington Goldsmith, N. Cvetojevic, M. Ireland, and S. Madden, "Fabrication tolerant chalcogenide mid-infrared multimode interference coupler design with applications for Bracewell nulling interferometry," *Opt. Exp.*, vol. 25, no. 4, pp. 3038–3051, 2017.

[19] J. Fernández *et al.*, "Statistical analysis of passive components manufactured in a thick silicon nitride platform (Student paper)," in *Proc. Eur. Conf. Integr. Opt.*, 2020.

[20] W. Bogaerts, Y. Xing, and U. Khan, "Layout-aware variability analysis, yield prediction, and optimization in photonic integrated circuits," *IEEE J. Sel. Top. Quantum Electron.*, vol. 25, no. 5, Sep./Oct. 2019, Art. no. 6100413.

[21] T. Han, "Nano-moulding of integrated optical devices," Ph.D. dissertation, Laser Phys. Centre, RSPE, The Australian National Univ., Canberra, ACT, Australia, 2011.

[22] J. C. Mikkelsen, W. D. Sacher, and J. K. S. Poon, "Dimensional variation tolerant silicon-on-insulator directional couplers," *Opt. Exp.*, vol. 22, no. 3, pp. 3145–3150, 2014.

[23] M. Gross, S. Dligatch, and A. Chtanov, "Optimization of coating uniformity in an ion beam sputtering system using a modified planetary rotation method," *Appl. Opt.*, vol. 50, no. 9, pp. C316–C320, Mar. 2011.

[24] E. A. J. Marcatili, "Dielectric rectangular waveguide and directional coupler for integrated optics," *Bell Syst. Tech. J.*, vol. 48, no. 7, pp. 2071–2102, 1969.

[25] N. Kumar, M. R. Shenoy, K. Thyagarajan, and B. P. Pal, "Graphical representation of the supermode theory of a waveguide directional coupler," *Fiber Integr. Opt.*, vol. 25, no. 3, pp. 231–244, 2006.

[26] I. D. Rukhlenko, M. Premaratne, and G. P. Agrawal, "Effective mode area and its optimization in silicon-nanocrystal waveguides," *Opt. Lett.*, vol. 37, no. 12, pp. 2295–2297, Jun. 2012.

[27] R. C. Gauthier, "Optical guided waves and devices," *Opt. Laser Technol.*, vol. 25, no. 2, 1993, Art. no. 146.

[28] S. Chen, Y. Shi, S. He, and D. Dai, "Low-loss and broadband 2×2 silicon thermo-optic Mach–Zehnder switch with bent directional couplers," *Opt. Lett.*, vol. 41, no. 4, pp. 836–839, 2016.

[29] D. Dai, "Advanced passive silicon photonic devices with asymmetric waveguide structures," *Proc. IEEE*, vol. 106, no. 12, pp. 2117–2143, Dec. 2018.

[30] S. J. Madden, M. Zhang, B. Luther-Davies, and R. Charters, "Patterning of inorganic polymer glass waveguiding films by dry etching," *Photon.: Des. Technol. Packag. III*, vol. 6801, 2007, Art. no. 680107.

[31] T. Han, S. Madden, M. Zhang, R. Charters, and B. Luther-Davies, "Low loss high index contrast nanoimprinted polysiloxane waveguides," *Opt. Exp.*, vol. 17, no. 4, pp. 2623–2630, 2009.

[32] R. C. Alferness and R. V. Schmidt, "Tunable optical waveguide directional coupler filter," *Appl. Phys. Lett.*, vol. 33, no. 2, pp. 161–163, 1978.